

Powerful method to evaluate the mass gaps of free-particle quantum critical systems

Francisco C. Alcaraz,^{1,*} José A. Hoyos,^{1,†} and Rodrigo A. Pimenta^{1,2,‡}

¹*Instituto de Física de São Carlos, Universidade de São Paulo,
Caixa Postal 369, 13560-970, São Carlos, SP, Brazil*

²*Departamento de Física, Universidade Federal de Lavras,
Caixa Postal 3037, 37200-000, Lavras, MG, Brazil*

(Dated: November 24, 2021)

We present a numerical method for the evaluation of the mass gap, and the low-lying energy gaps, of a large family of free-fermionic and free-parafermionic quantum chains. The method is suitable for some generalizations of the quantum Ising and XY models with multispin interactions. We illustrate the method by considering the Ising quantum chains with uniform and random coupling constants. The mass gaps of these quantum chains are obtained from the largest root of a characteristic polynomial. We also show that the Laguerre bound, for the largest root of a polynomial, used as an initial guess for the largest root in the method, gives us estimates for the mass gaps sharing the same leading finite-size behavior as the exact results. This opens an interesting possibility of obtaining precise critical properties very efficiently which we explore by studying the critical point and the paramagnetic Griffiths phase of the quantum Ising chain with random couplings. In this last phase, we obtain the effective dynamical critical exponent as a function of the distance-to-criticality. Finally, we compare the mass gap estimates derived from the Laguerre bound and the strong-disorder renormalization-group method. Both estimates require comparable computational efforts, with the former having the advantage of being more accurate and also being applicable away from infinite-randomness fixed points. We believe this method is a relevant tool for tackling critical quantum chains with and without quenched disorder.

Published in *Phys. Rev. B* **104**, 174206 (2021); DOI: [10.1103/PhysRevB.104.174206](https://doi.org/10.1103/PhysRevB.104.174206)

I. INTRODUCTION

Usually, the first step toward the understanding of an interacting many-body system relies on the study of a system in the absence of interactions, i.e., the free system. In particular, the study of free fermionic systems in the lattice, like the quantum Ising model or the quantum XY model, are excellent labs to probe new ideas and insights for magnetic systems [1, 2]. Free quantum systems with parafermionic degrees of freedom are also known in the literature, like the $Z(N)$ Baxter model [3, 4] and the multispin $Z(N)$ systems [5, 6].

A practical feature in the study of a free quantum chain is that the eigenvalues are given in terms of quasi-particle energies. The number of quasi-particle energies, normally calculated by a matrix diagonalization, grows linearly with the system's size. Since the computing time in the diagonalization procedure grows with powers of the system's size, typically we were able to deal only with systems with sizes up to $L = 5\,000 \sim 10\,000$. This is a problem in the cases where we need larger systems $L \sim 10^4$ or $L \sim 10^5$, or even for small chains in the case of quench disordered quantum chains since a large number of disorder configurations (typically 10^5) are necessary for achieving good statistics. A more severe constraint arises in quenched disordered systems since the diago-

nalization procedure suffers from numerical instabilities even for fairly small chains ($L \sim 100$) when the associated dynamical critical exponent is sufficiently large [7–9].

Frequently, we are interested only in the low-lying quasi-energies or, in the case of the mass gap evaluations, we only need the smallest free particle quasi-energy. We present in this paper a practical numerical method to evaluate the mass gaps, and possibly some of the low-lying energies within machine accuracy, and with a computational effort that increases only linearly with the size of the quantum chain. This method is based on the evaluation of a characteristic polynomial whose zeroes give the quasi-energies of the free-particle system. The calculation of all zeros of the polynomial requires the computation of all the coefficients of the polynomial, demanding a computer time that grows with powers of L . However, instead of calculating all the coefficients of the polynomial, in the method we propose in this paper, we only calculate a fixed number of them (C_{last}), independently of the system's size, demanding a computer time linearly proportional to L . These are the coefficients of the C_{last} larger powers in the polynomials.

The use of the simple secant method (or Newton's method) for the evaluation of the largest root of the characteristic polynomial, that gives us the mass gap, requires an initial guess for the root. We observed, for several free-fermionic and free-parafermionic quantum chains that the characteristic polynomial have only real roots, and the Laguerre bound (LB) [10–12], for the extreme roots, gives us an excellent approximation for the largest root. Differently from other bounds [10, 11] that normally re-

* alcaraz@ifsc.usp.br

† hoyos@ifsc.usp.br

‡ pimenta@ifsc.usp.br

quire the calculation of all the coefficients of the polynomial, the LBs are obtained only by using the three last coefficients. In the method we propose in this paper, this requires no extra computing time since we have already computed these coefficients.

Another advantage of the method we propose for the class of free-particle models we consider comes from the fact that the C_{last} -last coefficients of the characteristic polynomial of a quantum chain are already calculated from those of smaller lattice sizes. This means that with a little extra effort, we evaluate not only the mass gap of a quantum chain of size L but also the mass gaps of all the smaller ones. This is an enormous advantage of the method since normally for finite-size studies we need to calculate the mass gaps as a function of the system's size. The advantages of our method stems from the fact that it explores a general feature of the characteristic polynomial at criticality and in gapless phases: the largest root stands out from the remaining ones and dominates the LB.

Surprisingly, for the class of Hamiltonians we consider in this paper, the mass gaps obtained directly from the LB for the largest root of the characteristic polynomials, not only are close to the exact values of the largest roots, but also have the same finite-size dependence of the exact gaps. We observe that in the case of critical systems with uniform coupling constants, the LB gives us estimators for the dynamical critical exponent that coincide with the exact value.

As an application to quench disordered quantum chains, we consider the quantum Ising chain in a random transverse field. We study the model on its critical point as well on its Griffiths phase, which has a vanishing gap, even though not critical [13]. Surprisingly, our results indicate that the mass gap distributions derived from the LB are quite close to the exact ones. In the critical region, they give us the $z \rightarrow \infty$ value, and in the Griffiths phase the estimates for z are quite close to the ones derived from the numerically exact mass gap, obtained by the method we propose.

A largely used and important method for random systems ruled by the infinite-randomness renormalization-group fixed point is the so-called strong-disorder renormalization group (SDRG) method. This method allows, in the case of the quantum critical Ising systems, the exact evaluation of the dynamical critical exponent ($z \rightarrow \infty$). The case of finite systems, although not exact, gives us a reasonable estimate for the mass gaps of the quantum chains with large lattice sizes.

Since the method we propose in this paper gives the exact finite-size mass gap evaluations for quite large lattices ($L \sim 10^6$) within machine accuracy at criticality and in gapless phases, we also present a detailed comparison of the mass-gap distributions obtained from both, the SDRG and the LB.

Our analyses show that although the SDRG gives us good results, the mass gaps estimates coming from the LB are closer to the exact ones. We think that this obser-

vation will have an impact on future studies of quenched random systems, since the LB estimator are in general obtained with basically the same computational effort as compared with the SDRG.

Using standard brute force diagonalization methods, it is quite difficult to calculate the effective dynamical critical exponent z in the Griffiths phase, specially as we tend towards the critical point where $z \rightarrow \infty$. In this case, we need the mass gap evaluations for quite large lattices to get reliable results. As a test of our numerical method, we obtain this exponent by calculating the mass gaps for lattices of sizes $10^6 - 10^7$. This enables us the evaluation of large values of z , allowing us to study its dependence $z(\delta)$ with the distance from criticality δ .

The remainder of this paper is organized as follows. In Sec. II, we present the class of free-particle quantum chains suitable to the numerical method we propose in this paper. In Sec. III, we present our numerical method. In Sec. IV, we present some applications of the method to the homogeneous quantum critical Ising chain at the critical point and in the paramagnetic and ferromagnetic phases. We also apply the method to some generalizations of this model. We also provide a criterion which explains the success of the LB for estimating the mass gap. In Sec. V, we apply the method to the random transverse-field Ising chain at the critical point and in the paramagnetic Griffiths phase. A detailed comparison with the SDRG method is provided. Finally, in Sec. VI we summarize our conclusions. Some technical details on the SDRG method are given in the Appendix.

II. FREE-FERMIONIC AND FREE-PARAFERMIONIC QUANTUM CHAINS

The method we present in this paper is effective for the calculation of the mass gaps and some low-lying eigenenergies for models whose eigenspectra are given in terms of zeros of polynomials. This is the case at least for two general families of non-interacting Hamiltonians presented below. The method is shown to be efficient in the regions where the gap is small, as happens in critical regions or in the Griffiths phases of random systems. These are indeed the regions where the standard methods are less effective for large system sizes.

A. Models with $Z(N)$ symmetry

The first family is an infinite set of quantum chains with multispin interactions introduced in Refs. 5, 6. The free-fermionic Hamiltonians contain $(p + 1)$ -body interacting spins ($p = 1, 2, \dots$) and are given by

$$H^{(p)} = - \sum_{i=1}^p \lambda_i \sigma_i^x \prod_{j=1}^{i-1} \sigma_j^z - \sum_{i=p+1}^M \lambda_i \sigma_i^x \prod_{j=i-p}^{i-1} \sigma_j^z, \quad (1)$$

where $\sigma_i^{z,x}$ are spin-1/2 Pauli matrices attached to site i , M is the number of sites, and the coupling constants $\{\lambda_i\}$ are real numbers.

The case $p = 1$ is a simple nearest two-body interacting Hamiltonian

$$H^{(p=1)} = -\lambda_i \sigma_i^x - \sum_{i=2}^M \lambda_i \sigma_{i-1}^z \sigma_i^x, \quad (2)$$

which has the same eigenspectrum (apart for global degeneracy of the entire spectrum) as the quantum Ising chain

$$H_{\text{Ising}} = -\sum_{i=1}^{L-1} (h_i \sigma_i^x + J_i \sigma_i^z \sigma_{i+1}^z) - h_L \sigma_L^x - h_s \sigma_L^z, \quad (3)$$

where the transverse fields are $h_i = \lambda_{2i-1}$ and the coupling constants are $J_i = \lambda_{2i}$. The last term is a surface longitudinal field which is $h_s = 0$ when $M = 2L - 1$ and $h_s = \lambda_{2L}$ when $M = 2L$.

The model (1) with $p = 2$ recovers the three-spin interacting model introduced by Fendley [14]. Recently, the free-fermionic $Z(2)$ case has been generalized for Hamiltonians with certain frustration graphs [15].

This family of $Z(2)$ Ising models with multispin interactions are, in fact, particular cases of more general $Z(N)$ free-parafermionic models [5, 6] which are obtained by replacing the Pauli matrices in (1) by their $Z(N)$ generalizations: $\sigma^x \rightarrow X$, $\sigma^z \rightarrow Z$, where the algebra

$$XZ = \omega ZX, \quad X^\dagger = X^{N-1}, \quad Z^\dagger = Z^{N-1} \quad (4)$$

is obeyed, with $\omega = e^{i\frac{2\pi}{N}}$ and $X^N = Z^N = \mathbf{1}$. The case $p = 1$ recovers the free-parafermionic Baxter quantum chain [3].

As shown in Refs. 5, 6, the spectrum of all these quantum chains are obtained from the \bar{M} roots $\{z_i\}$ of the characteristic polynomial

$$P_M^{(p)}(z) = \sum_{\ell=0}^{\bar{M}} C_M(\ell) z^\ell, \quad (5)$$

with $\bar{M} = \text{int}\left(\frac{M+p}{p+1}\right)$ and $\text{int}(z)$ being the integer part of z , which obeys the following recurrence relation:

$$P_M^{(p)}(z) = P_{M-1}^{(p)}(z) - z \lambda_M^N P_{M-p-1}^{(p)}(z), \quad (6)$$

with the initial condition $P_j^{(p)}(z) = 1$ for $j \leq 0$. The polynomial $P_M^{(1)}(z)$ with arbitrary λ_M is connected to the FST polynomials [16, 17]. If $\lambda_M = 1$, the polynomial $P_M^{(1)}(z)$ is connected with the Chebyshev polynomial of the second type.

The *quasiparticle energies* $\{\varepsilon_i\}$ and the roots are related through $\varepsilon_i = z_i^{-\frac{1}{N}}$. Apart from degeneracies, the eigenenergies of these general free-fermionic ($N = 2$) or free-parafermionic ($N > 2$) quantum chains are given by

$$E_{\{s_1, \dots, s_{\bar{M}}\}} = -\sum_{i=1}^{\bar{M}} \omega^{s_i} \varepsilon_i, \quad (7)$$

where $s_i = 0, 1, \dots, N - 1$ and, as before, $\omega = e^{i\frac{2\pi}{N}}$. The ground-state energy $E_{\text{GS}} = -\sum_{i=1}^{\bar{M}} \varepsilon_i$ is obtained by taking $s_k = 0, \forall k$, and the low-lying energies are obtained changing the values of s_k for the k 's associated to the largest roots of $P_M^{(p)}(z)$. In particular, the mass gap $\Delta = (1 - \omega) z_{>}^{-\frac{1}{N}}$, where $z_{>} = \max\{z_i\}$.

We call attention to the important fact that the spectrum of the free-parafermionic quantum chain ($N > 2$) is not real. Nonetheless, it can be obtained from the polynomial (5) which possesses only real roots. In Sec. III, we present a numerical method suitable for calculating the largest roots of the polynomial.

B. Models with $U(1)$ symmetry

The second family of models that our method is effective for the evaluation of the mass gaps are generalizations of the XY quantum chains. The models are $U(1)$ -symmetric, i.e., the z component of the magnetization $S^z = \sum_i^L \sigma_i^z$ is a good quantum number. These Hamiltonians have a parameter q that, similarly as the first family of models we described, defines a special $(q + 1)$ -multispin interaction. They are given by

$$H^{(q)} = \sum_{i=1}^{L-1} \mu_i \sigma_i^+ \sigma_{i+1}^- + \sum_{i=1}^{L-q} \nu_i \sigma_i^- \left(\prod_{j=i+1}^{i+q-1} \sigma_j^z \right) \sigma_{i+q}^+, \quad (8)$$

where $\{\mu_i, \nu_i\}$ are the coupling constants and $\sigma^\pm = \frac{1}{2}(\sigma^x \pm i\sigma^y)$. In general, for $q > 1$, the models are non-Hermitian.

The case $q = 1$ gives us

$$H^{(q=1)} = \sum_{i=1}^{L-1} \mu_i \sigma_i^+ \sigma_{i+1}^- + \sum_{i=1}^{L-1} \nu_i \sigma_i^- \sigma_{i+1}^+. \quad (9)$$

It recovers the isotropic XY model for $\mu_i = \nu_i = 1$, the dimerized XY quantum chain with dimerization coupling δ for $\mu_i = \nu_i = (1 + (-)^i \delta)$, as well as general disordered XY quantum chains.

The Jordan-Wigner transformation [2] introduces the spinless fermionic operators

$$c_i = \sigma_i^- \prod_{j=1}^{i-1} \sigma_j^z, \quad c_i^\dagger = \sigma_i^+ \prod_{j=1}^{i-1} \sigma_j^z, \quad (10)$$

$i = 1, \dots, L$, satisfying the fermionic algebra $\{c_i, c_j^\dagger\} = \delta_{i,j}$, $\{c_i, c_j\} = 0$.

In terms of these operators, the Hamiltonian (8) has the bilinear form

$$H_{\text{fermion}}^{(q)} = - \sum_{i,j} c_i^\dagger \mathbb{A}_{i,j} c_j, \quad (11)$$

where the hopping matrix is

$$\mathbb{A}_{i,j} = \mu_i \delta_{j,i+1} + \nu_j \delta_{j,i-q}. \quad (12)$$

Although \mathbb{A} is not symmetric, it can still be transformed to the diagonal form

$$H_{\text{fermion}}^{(q)} = - \sum_k \Lambda_k \eta_k^\dagger \eta_k, \quad (13)$$

with $\{\eta_i, \eta_j^\dagger\} = \delta_{i,j}$, $\{\eta_i, \eta_j\} = \{\eta_i^\dagger, \eta_j^\dagger\} = 0$, and Λ_k being the k th eigenvalue of \mathbb{A} (which is, in general, complex). This is possible via the transformation

$$\eta_k = \sum_{i=1}^L \mathbb{L}_{i,k} c_i \quad \text{and} \quad \eta_k^\dagger = \sum_{i=1}^L \mathbb{R}_{i,k} c_i^\dagger, \quad (14)$$

where the columns of the \mathbb{L} and \mathbb{R} matrices are, respectively, the left and right eigenvectors of \mathbb{A} with the proper normalization $\mathbb{L}^T \mathbb{R} = \mathbb{1}$, which implies $\mathbb{R} \mathbb{L}^T = \mathbb{1}$.¹

Consequently, the 2^L eigenenergies of $H^{(q)}$ follows from the L -pseudo energies $\{\Lambda_k\}$:

$$E_{\{s_1, \dots, s_L\}} = - \sum_{k=1}^L \left(\frac{1 + (-1)^{s_k}}{2} \right) \Lambda_k, \quad (15)$$

with $s_k = 0$ or 1 .

The pseudo-energies $\{\Lambda_k\}$ are given by the roots of $\det(\Lambda \mathbb{1} - \mathbb{A}) = 0$. Equivalently, apart from zero modes ($\Lambda_k = 0$), $\{\Lambda_k\}$ are obtained from the zeros $\{z_k\}$ of the characteristic polynomial $P_L^{(q)}(z)$ given by

$$P_L^{(q)}(z) = \det(\mathbb{1} - z\mathbb{A}), \quad (16)$$

where $\Lambda_k = 1/z_k$.

The Laplace cofactor expansion for the determinant, when applied to our models, where \mathbb{A} is given by (12), produces the recurrence relation

$$P_L^{(q)} = P_{L-1}^{(q)} - z^{q+1} \left(\prod_{j=1}^{q-1} \mu_{L-j} \right) \mu_{L-q} \nu_{L-q} P_{L-q-1}^{(q)}, \quad (17)$$

for $L > q$, with the initial conditions

$$P_L^{(q)}(z) = 1, \quad (18)$$

for $1 \leq L \leq q$. This means that the eigenspectrum of (9) or (11) and (12) are functions only of the effective $L - q + 1$ couplings

$$\beta_0^{(q)} = \prod_{j=L-q+1}^{L-1} \mu_j, \quad \beta_i = \mu_i \nu_i, \quad (19)$$

($i = 1, \dots, L - q$), and we can rewrite the recurrence (17) as

$$P_L^{(q)}(z) = P_{L-1}^{(q)}(z) - \beta_0^{(q)} \beta_{L-q} z^{q+1} P_{L-q-1}^{(q)}(z). \quad (20)$$

Actually, in $P_L^{(q)}(z)$ only appears powers of z which are multiples of $(q + 1)$, i.e.,

$$P_L^{(q)}(z) \equiv Q_L^{(q)} = \sum_{\ell=0}^{\text{int}(\frac{L}{q+1})} a_L(\ell) r^\ell, \quad r = z^{q+1}. \quad (21)$$

For each root of r_j of $Q_L^{(q)}$ there are $(q + 1)$ roots of z_j , i. e., $z_j^{(k)} = r_j^{\frac{1}{q+1}} e^{i \frac{2\pi k}{q+1}}$ ($k = 0, 1, \dots, q$), that correspond to the non-zero fermionic quasi-energies Λ_k in (13).

The ground-state energy is given by $E_0 = - \sum_{j=0}^{\text{int}(L/(q+1))} z_j^{(0)}$, and the low-lying energies of (8) or (11) is obtained from the smallest roots r_j . In particular, the mass gap is obtained from the smallest non zero root \bar{r} , and its real part is given by $\text{Real}(\text{gap}) = \bar{r}^{-1/(q+1)} (1 + \cos(2\pi/(q+1)))$.

This means that the evaluation of the mass gaps of the two families of models, namely, the multispin free-fermionic models (1) and the generalized XY models (8), demands the calculation of the largest root of the polynomials (5) and (21). In the next section, we present a practical method to evaluate these roots.

III. A PRACTICAL METHOD FOR THE EVALUATION OF THE LARGEST ROOT OF THE POLYNOMIALS $P(z)$

For the family of polynomials with recurrence relations given in (6) and (20) the largest root can be obtained, for example, by the secant method where the roots of the polynomial $P(z)$ are obtained from the iteration

$$z^{(i+1)} = z^{(i)} - P(z^{(i)}) \frac{z^{(i)} - z^{(i-1)}}{P(z^{(i)}) - P(z^{(i-1)})} \quad (22)$$

or by the Newton method

$$z^{(i+1)} = z^{(i)} - \frac{P(z^{(i)})}{P'(z^{(i)})}. \quad (23)$$

The success of the method depends on two factors: (i) a good initial value for the largest root and (ii) an effective and precise way to evaluate $P(z)$ for values of z around the largest root.

¹ In other words, $\mathbb{A} \mathbb{R} = \mathbb{R} \mathbb{D}_\Lambda$ and $\mathbb{L}^T \mathbb{A} = \mathbb{D}_\Lambda \mathbb{L}^T$ with the diagonal matrix $(\mathbb{D}_\Lambda)_{i,j} = \Lambda_j \delta_{i,j}$.

We verified that, at least for the polynomials associated to the two interesting families of quantum chains presented in Sec. II, all the roots are real and a quite good guess for the largest root is given by the LB (see corollary 6.2.4 of Ref. 10) for the largest root of a polynomial. For the polynomials defined in (6), i.e.,

$$P_M(z) = \sum_{\ell=0}^{\bar{M}} C_M(\ell) z^\ell, \quad (24)$$

the LB for the largest root is given by

$$z_+ = -\frac{y_1}{\bar{M}} + \frac{\bar{M}-1}{\bar{M}} \sqrt{y_1^2 - 2 \left(\frac{\bar{M}}{\bar{M}-1} \right) y_2}, \quad (25)$$

where

$$y_1 = \frac{C_M(\bar{M}-1)}{C_M(\bar{M})}, \quad y_2 = \frac{C_M(\bar{M}-2)}{C_M(\bar{M})}. \quad (26)$$

It is important to mention that, differently from other bounds that demand the knowledge of all the coefficients $C_M(\ell)$ [10, 11], the LB only needs the last three ones, namely, $C_M(\bar{M})$, $C_M(\bar{M}-1)$ and $C_M(\bar{M}-2)$. As we shall see, in the applications of Secs. IV and V, this bound is not only a good estimate for the largest root of the polynomials of Sec. II, but also has the same leading finite-size dependence of the exact value of the largest root.

The evaluation of $P_M(z)$, by using the recurrence relation (6), takes a time that grows with $\mathcal{O}(M^2)$, and for $M \sim 10^6 - 10^7$ the coefficients are quite large requiring multiple precision (~ 1000 digits) to express them. However, we verified that the quantum chains (1), (8), and (11), in several interesting applications (see Secs. IV and V), have the last $C_{\text{last}} \sim 50$ coefficients of the higher power monomials, expressed with machine accuracy, by using standard 32-byte floating point (quadruple precision in FORTRAN computing language). These C_{last} coefficients could, in principle, be calculated directly, since they can be expressed in terms of the partition function of polymers in a line of M sites with local dependent fugacity [given by λ_i^N in (6)], and excluded volume of $(p+1)$ sites [5, 6]. However, the calculation time of these partition functions grows exponentially with M .

The recurrence relations (6) or (20) allow us to formulate a simple iteration procedure that gives us the last C_{last} coefficients of the polynomial. In Fig. 1, we show pictorially the procedure for the case $p = 1$ or $q = 1$ with initial conditions $P_{M \leq 0}(z) = \delta_{M,0}$.

Consider the recurrence (6). To save memory in the source-computing code for the coefficient evaluation, it is better to define the auxiliary coefficients $\{D\}$:

$$D([M-1]_{p+1}; \ell) \equiv C_M(\ell), \quad (27)$$

where $\ell = \bar{M} - C_{\text{last}}, \bar{M} - C_{\text{last}} + 1, \dots, \bar{M}$, $[M]_{p+1}$ denotes $M, \text{mod}(p+1)$, and as before $\bar{M} = \text{int}\left(\frac{M+p}{p+1}\right)$. We have the iteration procedure:

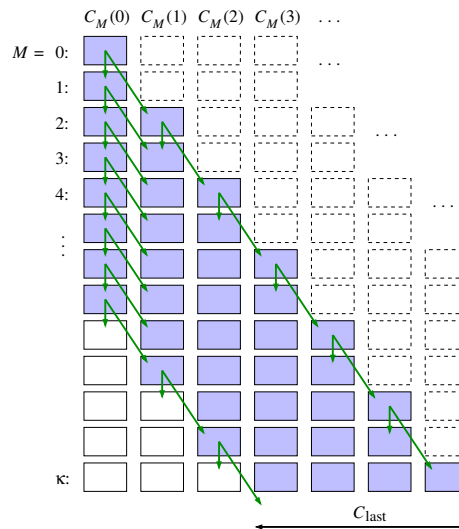


Figure 1. Schematic recursive procedure (6) for generating the coefficients of the polynomial for the case $p = 1$ and initial conditions $C_{m \leq 0}(\ell) = \delta_{m,0} \delta_{\ell,0}$. The ℓ th slot in the M th line represents the coefficient $C_M(\ell)$ in (24). Dashed slots represent non-existent coefficients. The arrows link a parent coefficient to their offsprings in accordance to (6). (For clarity, only a few arrows are shown.) If only the last C_{last} coefficients are needed in a given generation, say, κ , then only $\min\{C_{\text{last}}, \bar{M} + 1\}$ coefficients are needed in the previous ones (shaded slots).

For $M' = 1, \dots, C_{\text{last}}$,

$$D([M'-1]_{p+1}; j) = D([M'-2]_{p+1}; j) - \lambda_{M'}^N D([M'-1]_{p+1}; j-1), \quad (28)$$

for $j = M', M' - 1, \dots, 1$, with the initial condition

$$D(M'; j) = \delta_{j,0} \text{ for } 0 \leq M' \leq p, \quad (29)$$

and for $M' = C_{\text{last}} + 1, \dots, M$,

$$D([M'-1]_{p+1}; j) = D([M'-2]_{p+1}; j) - \lambda_{M'}^N D([M'-1]_{p+1}; j-1), \quad (30)$$

for $j = \bar{M}, \bar{M} - 1, \dots, \bar{M} - C_{\text{last}}$. The iteration (28)–(30) is a crucial step in our method to evaluate the mass gaps of quantum chains presented in Sec. II.

It is important to mention some interesting computational features of the iteration (28)–(30). (i) The number of operations, and hence the computing time, grows linearly with M . (ii) When calculating the polynomial coefficients for a given M , we have also to calculate the coefficients for all smaller quantum chains $M' < M$. (iii) The computing memory used in the procedure grows linearly with M . (iv) The coefficients necessary for the evaluation of the LB (25) and (26) are already calculated for all $M' \leq M$.

As a practical procedure, instead of calculating the largest root of $P_m(z)$, it is better to calculate its inverse

by searching the smallest root of the polynomial

$$\begin{aligned} \bar{P}_M(z) = z^{-\bar{M}} P_M(z) &= \sum_{\ell=0}^{C_{\text{last}}-1} C_M(\bar{M}-\ell) \frac{1}{z^\ell} \\ &+ \sum_{\ell=C_{\text{last}}}^{\bar{M}} C_M(\bar{M}-\ell) \frac{1}{z^\ell}. \end{aligned} \quad (31)$$

Our numerical results (see Sec. IV and V) show that for moderate values of the couplings [for example $\lambda^N \sim \mathcal{O}(1)$] in (5) the polynomial evaluation in (31) for values of z around the LB, already converges with precision $10^{-25} - 10^{-30}$ by taking $C_{\text{last}} \sim 40 - 50$ terms. The predicted gap will have a precision of $10^{-22} - 10^{-25}$, for polynomials with $M \sim 10^6 - 10^7$. Actually the appropriate choice of the number C_{last} of coefficients in the iteration procedure (28)-(30) is obtained by imposing that $|C_M(\bar{M}-C_{\text{last}})(1/z)^{C_{\text{last}}}| < 10^{-31} - 10^{-32}$, giving us the standard precision of 32 bytes numerical precision (quadruple precision in FORTRAN codes). During the iteration of the secant method (22), with the successive evaluation of (31) we can check if this precision is reached.

In the next section, we will present some applications of the numerical method we proposed in this paper.

IV. MASS GAP OF CLEAN SYSTEMS

In this section, we apply the numerical method introduced in Sec. III to the family models (1) in the case of homogeneous critical and off-critical systems, and benchmark the numerical results against analytically exact ones whenever possible.

A. The critical chain

A good initial test is the critical TFI chain (3) ($h_i = J_i = 1$). The corresponding pseudo-energies are

$$\varepsilon_k = 2 \sin \left(\frac{2k+1}{4L+2} \pi \right), \quad k = 0, 1, \dots, L-1, \quad (32)$$

and

$$\varepsilon_k = 2 \sin \left(\frac{k\pi}{2L+2} \right), \quad k = 1, \dots, L, \quad (33)$$

when the surface longitudinal field is $h_s = 0$ and $h_s = 1$, respectively. The corresponding mass gaps are, respectively, $\Delta_{\text{analytic}} = 2\varepsilon_0$ and $2\varepsilon_1$.

We start by computing the truncated polynomial (31) via the recurrence relation (6) from which we obtain the largest root $z_>$ using the standard Newton's method using the upper LB z_+ (25) as an initial guess.² The cor-

² We have also used the secant method and obtained the same numerical result without noticing any significant change in the computational time.

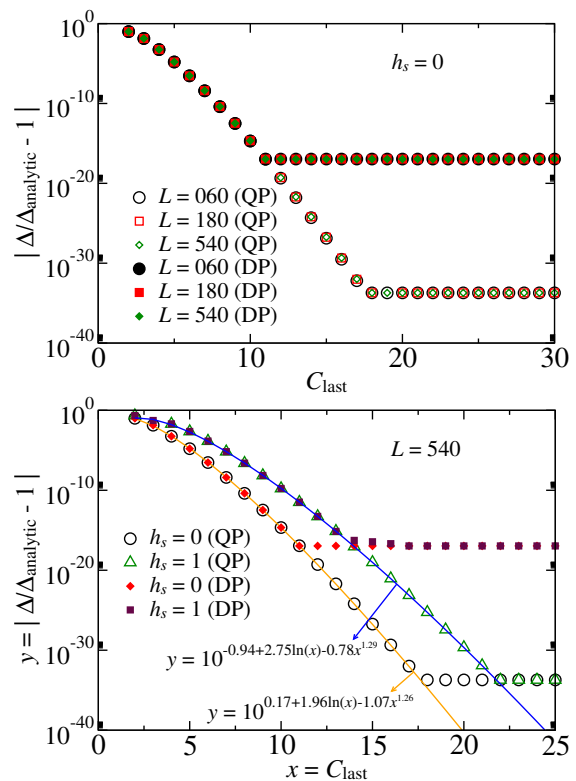


Figure 2. The relative difference between the numerical Δ and analytical Δ_{analytic} mass gaps of the quantum critical Ising chain (3) ($h_i = J_i = 1$) with the former being computed from the characteristic polynomial truncated with C_{last} coefficients (31). In the top panel, three different chain lengths L and two different numerical precisions are considered for the case without longitudinal surface field $h_s = 0$. In the bottom panel, the cases with ($h_s = 1$) and without ($h_s = 0$) longitudinal fields are shown for different numerical precisions and $L = 540$. DP and QP stand for double and quadruple precision in FORTRAN codes, respectively. The solid lines are simple fits of the data.

responding mass gap is simply $\Delta = 2/\sqrt{z_>}$. This procedure is performed using standard double and quadruple precision in FORTRAN computing language (16 and 32 significant digits, respectively). The results are plotted in Fig. 2. In the top panel, we consider the standard case $h_s = 0$ with chains of size $L = 60, 180$, and 540 . As can be noted, the mass gap can be accurately computed with standard FORTRAN quadruple precision using the characteristic polynomial truncated to $C_{\text{last}} \approx 20$ terms for all system sizes. In the bottom panel, we compare the cases $h_s = 0$ and $h_s = 1$. As can be seen, the latter requires a few more terms in the truncated polynomial ($C_{\text{last}} \approx 25$) to compute the mass gap within quadruple precision.

In sum, to compute the mass gap of the clean critical model (3) with precision of one part in 10^{32} , only a few terms in the characteristic polynomial is required.

As a further numerical test, we calculated the mass gaps Δ for lattice sizes up to $L = 1.2 \times 10^6$, keeping

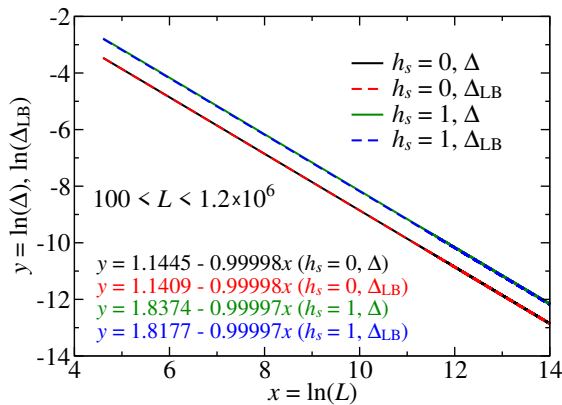


Figure 3. The finite-size mass gap Δ of the quantum critical Ising chain (3) ($h_i = J_i = 1$) with ($h_s = 1$) and without ($h_s = 0$) a longitudinal surface field for lattice sizes $L = 100, 200, \dots, 1.2 \times 10^6$. The Laguerre bound estimate [$\Delta_{\text{LB}} = 2/\sqrt{z_+}$, see Eq. (25)] is also shown. Linear fits to the entire data are provided in the panel.

only the first $C_{\text{last}} = 50$ coefficients of the characteristic polynomial.³ The finite-size gap is shown in Fig. 3 as a function of the lattice size L for both cases with and without the longitudinal surface field. It is well-known that $\Delta \sim L^{-z}$ with a dynamical critical exponent $z = 1$. Standard linear regression of the data gives us the exponent $z = 0.9999 \approx 1$.

We now call attention to the fact that the upper LB provides an interesting estimate to the mass gap. Let this estimate be $\Delta_{\text{LB}} \equiv 2/\sqrt{z_+}$, where z_+ is the upper bound in (25). As also shown Fig. 3, Δ_{LB} shares the same finite-size scaling as the exact mass gap, i.e., $\Delta_{\text{LB}} \sim L^{-z_{\text{LB}}}$, with $z_{\text{LB}} = z = 1$. Actually, this numerical finding is shown to be analytically correct for the entire family of models (1) in the homogeneous case. For $J_i = h_i = 1$, the coefficients $C_M^{(p)}(\ell)$ are given by the binomial [5, 6]

$$C_M^{(p)}(\ell) = \binom{M-p(\ell-1)}{\ell}, \quad (34)$$

with $\ell = 0, 1, \dots, \bar{M}$. For $M \approx \bar{M}(p+1) - p \gg p$, the upper LB (25) diverges as $z_+ \sim \bar{M}^{p+1} \sim L^{p+1}$. Therefore, $\Delta_{\text{LB}} \sim L^{-z_{\text{LB}}}$, with

$$z_{\text{LB}} = \frac{p+1}{2} = z, \quad (35)$$

³ This is more than necessary for the clean critical system, but it is convenient for disordered systems as different configurations converge differently (see Sec. V). In practice, we do not compute all the C_{last} terms of the \bar{P}_M (31) when iterating root-finding method (22) or (23) since we do not need \bar{P}_M with ϵ precision. We need to compute $\Delta z^{(\alpha)}/z^{(\alpha)}$ with ϵ -precision since we want $z >$. It is then convenient to compute an initial estimate of $\Delta z^{(\alpha)}/z^{(\alpha)}$ with only a few terms (less than C_{last}) in the sum of \bar{P}_M (and its derivative in the case of the Newton's method) and then improve it by adding further terms in the sum until the desired precision is reached.

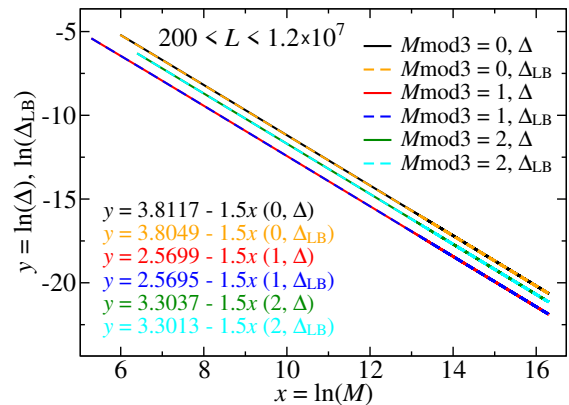


Figure 4. The mass gap Δ and the associate Laguerre's bound estimate Δ_{LB} of the quantum critical chain (1) with $p = 2$ at the isotropic point ($\lambda_i = 1$) and lattice sizes $200 < M < 1.2 \times 10^7$. The results are divided into three sets of curves according to the value of $M \bmod 3$. Best linear fits to the entire data are provided in the panel.

which coincides with the dynamical exponent [5, 6].⁴

For completeness, we compare the value of Δ_{LB} with the exact one [either (32) or (33)]. By expanding the binomial (34) for $M \gg p$, it is easy to show that, for $h_s = 0$ and $p = 1$, $\Delta_{\text{LB}} = (0.9964 + 0.0126L^{-1} - 0.0063L^{-2} + \dots) \Delta$ and, for $h_s = 1$ and $p = 1$, $\Delta_{\text{LB}} = (0.9804 - 0.0828L^{-1} - 0.0612L^{-2} + \dots) \Delta$.

We now apply our method to the case $p = 2$ of the model in (1) at the multi-critical point ($\lambda_i = 1$). We verified that keeping $C_{\text{last}} = 50$ terms in the truncated polynomial is more than enough to ensure that we have computed its exact value (within standard FORTRAN quadruple precision) near the upper LB for all the lattice sizes studied. In Fig 4, we show the finite-size gap Δ for $200 < M < 1.2 \times 10^7$. The results are divided into three curves, depending on the value of $M \bmod 3$. The leading finite-size scaling behavior of Δ is known exactly [5, 6, 14] to be $\Delta \sim 1/M^z$, with $z = 3/2$ [as anticipated in (35)]. Our numerics are in perfect agreement with it.

We mention that in each curve of Figs. 3 and 4, respectively, 6×10^4 and 1.2×10^5 mass gaps were evaluated. Each curve took, respectively, around only two and twelve seconds of CPU time of a regular portable computer.

B. Further quasi-particle energies

Let us consider the extension of the method presented in Sec. III for evaluating the other low-lying gaps. The

⁴ For the case of $Z(N)$ free-parafermions with $p+1$ multi-spin interactions, Eq. (35) generalizes to $z_{\text{LB}} = \frac{p+1}{N}$.

expressions (32) and (33) for the energies provide an analytical reference for our numerical values. We proceed as follows. After the numerical evaluation of the largest root $z_>$ (using the upper LB z_+ as an initial value) of the characteristic polynomial P_M , the quotient polynomial,

$$Q_M(z) = \frac{P_M(z)}{z - z_>} = \sum_{\ell=0}^{\bar{M}-1} D_M(\ell) z^\ell, \quad (36)$$

provide us the next largest root. As the roots of Q_M are all real, the upper LB can be used. The new coefficients $D_M(\ell)$ are obtained recursively from, namely,

$$D_M(\bar{M} - j) = C_M(\bar{M} - j + 1) + z_> D_M(\bar{M} - j + 1), \quad (37)$$

with the initial condition $D_M(\bar{M} - 1) = C_M(\bar{M})$. The evaluation of the largest root of $Q_M(z)$ gives us the next mass gap $2\varepsilon_1$ in (32) or $2\varepsilon_2$ in (33). Iterating this procedure from $j = 2$ to \bar{M} provides us the other low-lying mass gaps. By keeping $C_{\text{last}} = 50$ terms in the truncated polynomial, we were able to obtain with precision higher than one part in 10^{15} the lowest nine pseudo-energies in (32) and (33) for lattice sizes $L \sim 10^6$. In other words, we have obtained the lowest $2^9 = 512$ eigenvalues of the system model (3).

C. Off-critical chain

We now study the applicability of our method to the off-critical TFI chain (3) with $h_i = 1$, $J_i = J$ (which we tune across the transition at $J_c = 1$).

Analogous to Fig. 2, we plot in Fig. 5 the relative difference between the mass gaps Δ and Δ_{analytic} as a function of C_{last} . The former is computed using the procedure defined in Sec. III, i.e., with standard FORTRAN quadruple precision using the truncated function (31) taking the last C_{last} terms. The latter is obtained from the generalizations (32) and (33), which are

$$\varepsilon_k = 2\sqrt{1 + 2J \cos q_k + J^2}, \quad (38)$$

where the values of the quasimomenta q_k depend on the value of h_s . The system gap is $\Delta_{\text{analytic}} = 2\varepsilon_F$, where ε_F is the quasi-energy associated to the closest q_k to π .

For $h_s = 0$, q_k are the roots of the equation

$$\sin((L+1)q) = -J \sin(Lq). \quad (39)$$

For $J \leq 1 + L^{-1}$, there are L real roots inside the interval $(0, \pi)$. The largest one is responsible for the system gap and is $q_F = \pi \left(1 - ((1+J)L)^{-1} + \mathcal{O}(L^{-2})\right)$.

For $J > 1 + L^{-1}$, there are $L - 1$ roots inside that interval. The remaining one is complex, yielding a gap that vanishes exponentially with the lattice size, which signals the spontaneous symmetry-breaking phenomena

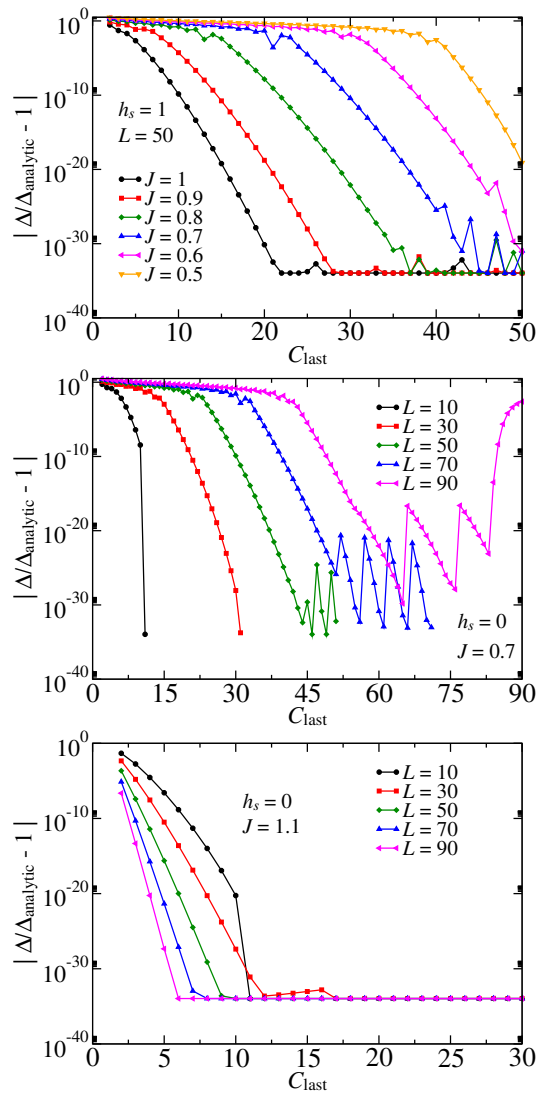


Figure 5. The relative difference between the exact mass gap Δ_{analytic} and the one Δ computed with standard FORTRAN quadruple precision (32 digits) using the truncated polynomial (31) with C_{last} terms. The model is the transverse-field Ising chain (3) with $h_i = 1$ and $J_i = J$ and longitudinal surface field h_s . Different values of J and h_s are indicated in the panels.

that happens in the thermodynamic limit of the ferromagnetic phase.⁵

For $h_s = 1$, the situation is much simpler since $q_k = \pi k/(L+1)$ [6]. In this case, there is no ordered phase. Both regions $J > 1$ and $J < 1$ are of the same disordered nature, a consequence of the exact duality of the model's eigenspectrum: $\varepsilon_k(J) = J\varepsilon_k(1/J)$ for all levels and lattice sizes.

⁵ For $L \gg 1$, the complex root is $q_F = \pi + iv$, with v satisfying $\sinh((L+1)v) = J \sinh(Lv)$, and yields the gap $\varepsilon_F = J^{1-L} \sqrt{1 - 2J^{-2} + \dots}$.

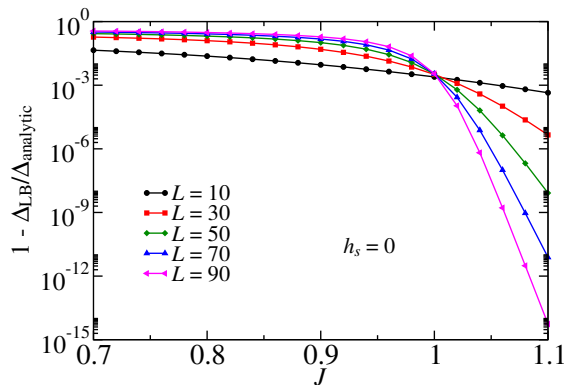


Figure 6. The relative difference between the analytic known gap Δ and the upper Laguerre's bound estimate Δ_{LB} as a function of the coupling constant J for the transverse-field Ising chain (3) ($h_i = 1$, $J_i = J$, and $h_s = 0$) and for different system sizes L .

As can be seen in the top and middle panels of Fig. 5, the farther inside the paramagnetic phase ($J < 1$) the more coefficients are needed in the truncated polynomial to obtain the same desired precision. This result is not unexpected. As the system is gapped, the largest roots of the polynomial (5) are close and, thus, the truncation procedure becomes less precise. The larger the system size L , the denser are the roots and, therefore, worse becomes the truncation approximation. For $L = 90$ and $J = 0.7$ (middle panel), the coefficients are so large for $C_{\text{last}} > 60$ that they cannot be accurately computed in quadruple precision. As a result, the entire method breaks down.

On the other hand, deeper inside the ferromagnetic phase ($J > 1$, see bottom panel of Fig. 5) the fewer coefficients are needed. This is also expected because the largest root of the polynomial (related to the exponentially small gap between the two nearly degenerated ground-states) diverges while the other ones remain finite. Hence, the truncation approximation becomes better and better as L increases.⁶

As previously mentioned, the upper LB already gives an interesting estimate for the system gap $\Delta_{\text{LB}} = 2/\sqrt{z_+}$. In Fig. 6, we plot the relative difference between Δ_{analytic} and Δ_{LB} as a function of J for various system sizes L . In the paramagnetic phase ($J < 1$), Δ_{LB} is a somewhat good estimate which worsens slightly as L increases and the system moves deeper inside the paramagnetic phase. At criticality, $\Delta_{\text{LB}} \approx (0.99 + \mathcal{O}(L^{-1}))\Delta$ as we have already discussed. On the other hand, Δ_{LB} is an excellent estimate when $L \rightarrow \infty$ in the ferromagnetic phase.

⁶ The usual gap related to the correlation length is the next higher level.

D. The suitability of Laguerre's upper bound

These results can be understood in the following way. Recasting the polynomial (5) as $P(z) = A \prod_{i=1}^{\bar{M}} (z - z_i)$, where $A \neq 0$ is an unimportant constant and $\{z_i\}$ are the roots, the Laguerre's upper bound (25) is simply $z_+ = \bar{z} + \sqrt{(\bar{M} - 1)\sigma_z^2}$, where $\bar{z} = \bar{M}^{-1} \sum_{i=1}^{\bar{M}} z_i$ is the average value of the roots and $\sigma_z^2 = \bar{z}^2 - \bar{z}^2$ is the associated variance [12]. We now separate the largest roots from the others. Let $\{\zeta_i\}$ ($i = 1, \dots, \bar{M} - 1$) be set of roots $\{z_i\}$ except that it does not contain the largest one $z_>$. Then $\bar{z} = \bar{M}^{-1} (z_> + (\bar{M} - 1)\bar{\zeta})$, with $\bar{\zeta} = (\bar{M} - 1)^{-1} \sum_{i=1}^{\bar{M}-1} \zeta_i$ being the average value of $\{\zeta_i\}$, and $\sigma_z^2 = (\bar{M} - 1) (z_>^2 - 2z_>\bar{\zeta} + \bar{\zeta}^2) = (\bar{M} - 1) (z_> - \bar{\zeta})^2$. The upper LB can be rewritten as

$$z_+ = \frac{z_>}{\bar{M}} + \left(1 - \frac{1}{\bar{M}}\right) \left(\bar{\zeta} + \sqrt{(z_> - \bar{\zeta})^2}\right). \quad (40)$$

If $z_> \gg \sigma_\zeta$, where $\sigma_\zeta^2 = \bar{\zeta}^2 - \bar{\zeta}^2$ is the variance of $\{\zeta_i\}$, the right-hand-side of (40) is dominated by the second term and, thus,

$$z_+ \approx z_> + \frac{\sigma_\zeta^2}{2z_>}. \quad (41)$$

This explains the success of Δ_{LB} in estimating Δ_{analytic} at the ferromagnetic phase, as $L \rightarrow \infty$, $z_> \rightarrow J^{2(\bar{M}-1)}$ while $\sigma_\zeta^2 \rightarrow \text{const}$. At the paramagnetic phase, both $z_>$ and σ_ζ tend to constants as $L \rightarrow \infty$ and, thus, Δ_{LB} does not improve as L increases. At criticality, the largest root increases as $z_> \sim L^{2z}$, with z being the dynamical exponent. Recall from the discussion below (35) that $\Delta_{\text{LB}} \approx (0.99 + \mathcal{O}(L^{-1}))\Delta$ does not improve as L diverges. This is because there are other roots which diverge likewise. Although they are a small subset of the entire set of roots $\{\zeta_i\}$, their divergence dominates the average and variance yielding $\sigma_\zeta \sim L^{4z}$. The important fact is that the divergence of $\sigma_\zeta^2/z_>$ cannot be greater than the divergence of $z_>$ itself. This fact generically ensures that $z_+ \sim L^{2z}$ and, therefore, $z_{\text{LB}} = z$.

V. THE MASS GAPS OF QUANTUM CHAINS WITH QUENCHED DISORDER

Reliable numerical results for quantum chains in the presence of quenched disorder are rare, especially for those exhibiting infinite-randomness criticality. The use of standard methods such as matrix diagonalization suffers from numerical instabilities even for moderate lattice sizes [9]. In this section, we apply our method to the random transverse-field Ising chain to illustrate its effectiveness and practicality. We obtain reliable numerical results for chain sizes up to $L \sim 10^7$ without much numerical effort.

A. Model and brief review

The system Hamiltonian is given by Eq. (3) where, for simplicity, we take the transverse fields to be uniform, $h_i = 1$. The coupling constants J_i are independent and identically distributed random variables. For simplicity, we take them uniformly distributed within the interval $0 < J_i < J_{\max}$, with J_{\max} playing the role of a tuning parameter across the quantum phase transition. We will not explore other possible disorder distributions as this is not the scope of this paper.

Before reporting our results, a review of few concepts is in order. We adopt the definition of Ref. 13 for the distance from criticality

$$\delta \equiv \frac{\overline{\ln h} - \overline{\ln J}}{\sigma_{\ln h}^2 + \sigma_{\ln J}^2} = 1 - \ln J_{\max}, \quad (42)$$

where $\overline{\dots}$ denotes the disorder average and $\sigma_x^2 \equiv \overline{x^2} - \overline{x}^2$ is the variance. Thus, the critical point happens for $J_{\max} = J_c = e$. Here, we will focus on finite-size gap Δ at the quantum critical point, $\delta = 0$, and on the Griffiths paramagnetic phase, $0 < \delta < 1$. At criticality, the leading finite-size scaling behavior of the typical value of the gap, $\Delta_{\text{typ}} = \exp(\overline{\ln \Delta})$, is of activated type, i.e., $\ln \Delta_{\text{typ}} \sim -L^\psi$, with a universal tunneling exponent $\psi = \frac{1}{2}$ [13]. Thus, the corresponding dynamical exponent is formally infinite. In addition, the distribution of the variable

$$\eta = \frac{\ln(2J_{\max}/\Delta)}{\sigma_0 L^\psi} \quad (43)$$

is L independent for sufficiently large system sizes $L \gg 1$. Here $\sigma_0 = \sqrt{\frac{1}{2}\sigma_{\ln h}^2 + \frac{1}{2}\sigma_{\ln J}^2} = \frac{1}{\sqrt{2}}$. The actual distribution of η is not analytically known, only an estimate based on a strong-disorder renormalization-group approach which is [18, 19]

$$\begin{aligned} \mathcal{P}_{\text{SDRG}}(\eta) &= \frac{4}{\sqrt{\pi}} \sum_{k=0}^{\infty} (-1)^k \left(k + \frac{1}{2}\right) e^{-\eta^2(k+\frac{1}{2})^2}, \\ &= \frac{4\pi}{\eta^3} \sum_{k=0}^{\infty} (-1)^k \left(k + \frac{1}{2}\right) e^{-\pi^2(k+\frac{1}{2})^2/\eta^2}. \end{aligned} \quad (44)$$

At the off-critical paramagnetic Griffiths phase, the system is still gapless. The typical value of the finite-size gap vanishes as $\Delta_{\text{typ}} \sim L^{-z}$ with a dynamical exponent that depends on the distance from criticality. Its exact value is known to be the root of $(J/h)^{\frac{1}{z}} = 1$ taken to its absolute value [20]. For the distributions here used and for $0 < \delta < 1$, the dynamical exponent is the root of the transcendental equation

$$z + 1 = ze^{\frac{1-\delta}{z}}, \quad (45)$$

which diverges as $z \approx \frac{1}{2\delta}$ for $\delta \ll 1$ [13].

B. Numerical precision

As in Sec. IV, we start by showing that the truncated polynomial (31) up to $C_{\text{last}} = 50$ is more than sufficient for obtaining the mass gaps with standard FORTRAN quadruple precision (32 significant digits). Unfortunately, the mass gap is not analytically known for a given disorder realization of the coupling constants. Thus, we define as the exact value the one obtained from the largest root of the truncated polynomial with $C_{\text{last}} = 50$ coefficients. The resulting mass gap is denoted by Δ_{exact} . In Fig. 7, we plot the relative difference between the gap obtained with fewer coefficients ($C_{\text{last}} \leq 40$) and Δ_{exact} for five different disorder configurations (chosen at random) for critical chains ($\delta = 0$) of sizes $L = 20, 40$, and 80 . As observed in the homogeneous chains (Sec. IV), $C_{\text{last}} = 50$ is more than enough for convergence and precision for any L .

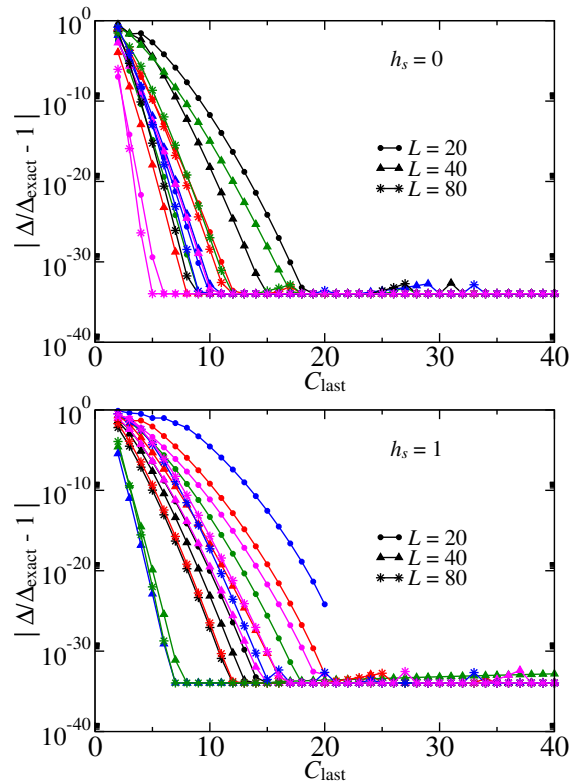


Figure 7. The relative difference between the numerical Δ and (see text) virtually exact Δ_{exact} mass gaps of the quantum critical Ising chain (3) with quenched disorder ($\delta = 0$) when the former is computed from the characteristic polynomial truncated with C_{last} coefficients (31). We show the results for chains of sizes $L = 20$ (circles), 40 (triangles), and 80 (stars), for five distinct disorder realizations (different colors), and for the cases without ($h_s = 0$, top) and with ($h_s = 1$, bottom) longitudinal surface fields. The solid lines are simple guides to the eyes.

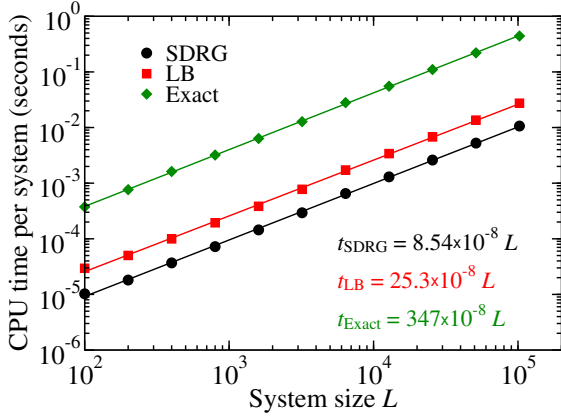


Figure 8. The CPU time required for computing the mass gap Δ as a function of the system size L . The chain is critical $\delta = 0$ and for $h_s = 0$. The data is averaged over 10^3 different disorder realizations. The program was coded in FORTRAN with standard quadruple precision and run on a conventional portable computer. Best power-law fits for the data (solid lines) are provided in the panel.

C. Numerical performance

We now study the numerical performance of our method. For such, we compute the exact value of the mass gap (truncating the characteristic polynomial up to $C_{\text{last}} = 50$) $\Delta = 2/\sqrt{z_-}$ for chain sizes ranging from $L = 100$ to 102400. We have used a conventional portable computer and coded in standard FORTRAN with quadruple precision. The required CPU time t_{Exact} is averaged over 1000 disorder realizations at criticality ($\delta = 0$) and $h_s = 0$. Our results are plotted in Fig. 8. As expected, the required time increases only linearly with L . It is interesting to note that less than a second is required even for chains of $L \sim 10^5$ sites. For comparison, we also plot the CPU time required for computing two estimates for the mass gap: the SDRG estimate Δ_{SDRG} (as explained in the Appendix), and the LB estimate $\Delta_{\text{LB}} = 2/\sqrt{z_+}$. As expected, the required CPU time for these two methods (t_{SDRG} and t_{LB} , respectively) also increases linearly with L . Note that $t_{\text{Exact}} \approx \frac{\ell_{\text{max}}}{3} t_{\text{LB}}$ since computing the LB requires the determination of the characteristic polynomial truncated at $C_{\text{last}} = 3$. Interestingly, note that t_{LB} is not much different from t_{SDRG} , a procedure that is arguably the fastest one for capturing the physics of the problem. (Finally, we report that quantitatively similar results were obtained for $h_s = 1$.)

D. Laguerre's upper bound as an estimate for the mass gap

We now explore the idea of using the Laguerre's upper bound (25) for estimating the mass gap, $\Delta_{\text{LB}} = 2/\sqrt{z_+}$. Therefore, we study its relative distance from the actual mass gap defined as $\alpha_{\text{LB}} = 1 - \Delta_{\text{LB}}/\Delta$ (recall that

$\Delta_{\text{LB}} < \Delta$). For comparison, we also study $\alpha_{\text{SDRG}} = \Delta_{\text{SDRG}}/\Delta - 1$ (we verified that $\Delta_{\text{SDRG}} > \Delta$). Our results are shown in Fig. 9. In the top panel, we plot the distribution W of α_{SDRG} for the critical chains ($\delta = 0$) for surface field $h_s = 0$ (main panel) and $h_s = 1$ (inset). Typically, the SDRG estimate for the mass gap is more than twice the actual value ($\bar{\alpha}_{\text{SDRG}} \gtrsim 1$). In addition,

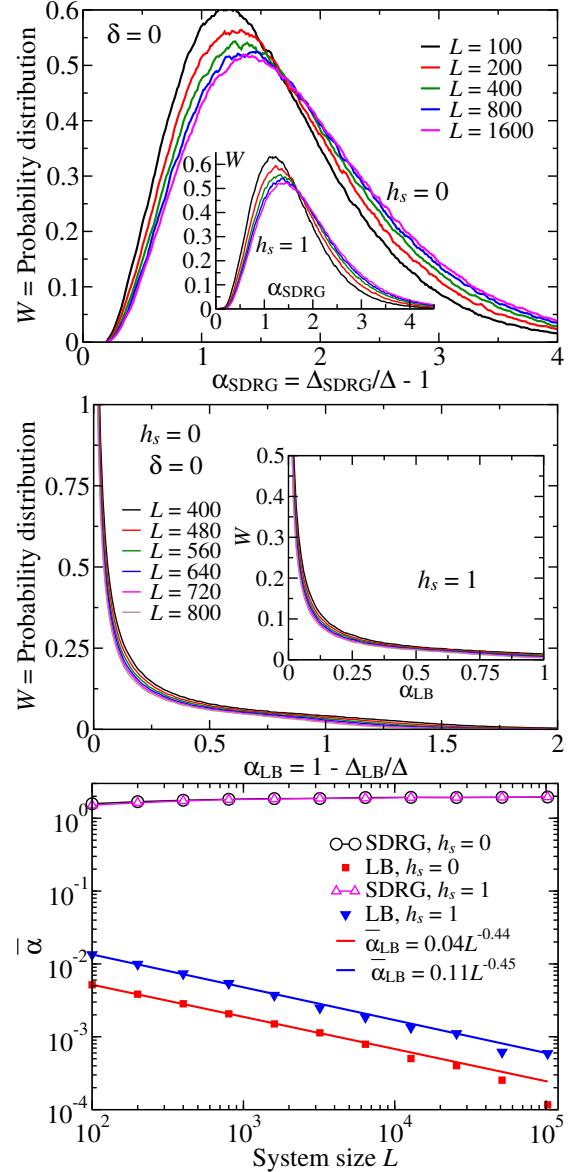


Figure 9. The top (middle) panel shows the probability distribution W of the relative difference α_{SDRG} (α_{LB}) between the finite-size gap Δ and the corresponding SDRG (Laguerre's bound) estimate Δ_{SDRG} (Δ_{LB}), for different system sizes L . The chains are critical ($\delta = 0$) and the surface longitudinal field is $h_s = 0$ (main panel) or $h_s = 1$ (inset). Each curve was constructed using 10^6 distinct disorder realizations. Bottom: The mean values of α_{SDRG} and α_{LB} as a function of L . Power-law best fits are provided for $\bar{\alpha}_{\text{LB}}$ (solid lines). Solid lines for $\bar{\alpha}_{\text{SDRG}}$ are simple guides to the eyes.

the SDRG estimate does not improve with increasing L . Actually, it worsens a little bit and saturates for large L (see bottom panel). The LB estimate, on the other hand, behaves quite differently (see middle panel). The distribution W is singular at the origin meaning that Δ_{LB} is a good estimate for Δ . In addition, the larger the system size the more singular is W at the origin. As shown in the bottom panel, the estimate Δ_{LB} becomes better with increasing L for the system sizes studied.

E. The distribution of mass gap at criticality

We now study the distribution of mass gap Δ and the corresponding LB estimate Δ_{LB} at criticality. When properly rescaled [see Eq. (43)], the distribution is expected to be L independent for $L \rightarrow \infty$. This is confirmed by our numerics as shown in Fig. 10. As could be anticipated by the results in Fig. 9 (middle and bottom panels), the distributions of Δ and Δ_{LB} are indistinguishable for large L since their intrinsic width grows with the system size while the relative difference between Δ and Δ_{LB} diminishes. For comparison, we also show the SDRG result. For $h_s = 0$, this is known analytically for $L \rightarrow \infty$, see Eq. (44). For $h_s = 1$, an analytical estimate is not available (to the best of our knowledge). We, therefore, compute it numerically. We have used 10^6 different disorder realizations of chains of size $L = 800$. Remarkably, these rescaled distributions \mathcal{P} are different for $h_s = 0$ and 1. This is unexpected since the difference is only an additional surface longitudinal field. We verified that a simple change of variables $\eta \rightarrow \text{const} \times \eta$ does

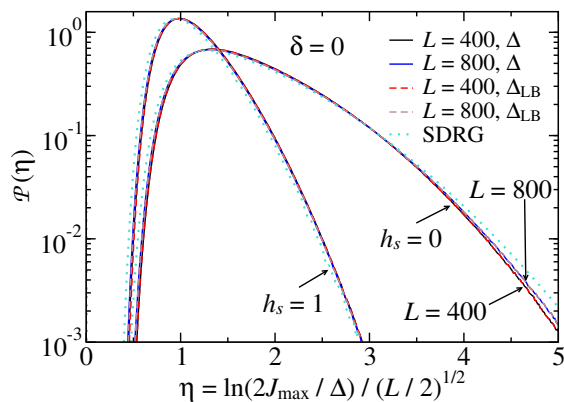


Figure 10. The distribution of the rescaled mass gap η (43) of the random transverse-field Ising chain at criticality $\delta = 0$ without surface field $h_s = 0$ for lattice sizes $L = 400$ and 800 . Both the exact value of the mass gap Δ and the Laguerre bound estimate Δ_{LB} are considered. Both distributions are statistically identical within our accuracy. Each curve was obtained from 1.1×10^8 distinct samples. The dotted line is the analytic strong-disorder renormalization-group estimate Eq. (44) for $h_s = 0$ while for $h_s = 1$ it is the numerical implementation of the SDRG method for 10^6 chains of size $L = 1600$.

not bring $\mathcal{P}_{h_s=0} \rightarrow \mathcal{P}_{h_s=1}$. In addition, we verify that the distribution \mathcal{P} does not converge to $\mathcal{P}_{\text{SDRG}}$ in the thermodynamic limit. We verify from Fig. 10 that the high-gap tail of \mathcal{P} is fully converged and different from that of $\mathcal{P}_{\text{SDRG}}$. This can be interpreted as a consequence of the results in the top panel of Fig. 9 where the peak of $W(\alpha_{\text{SDRG}})$ shifts away from zero as L increases.

F. The dynamical critical exponent in the paramagnetic Griffiths phase

Another interesting test to the numerical method of Sec. III is the evaluation of the effective dynamical critical exponent z in the Griffiths paramagnetic phase of the quantum chain (3). As briefly reviewed in Sec. V A, the system is not critical although gapless. We, therefore, compute the finite-size gap Δ (and the LB estimate Δ_{LB}) and study its typical value, i.e., $\Delta_{\text{typ}} \equiv \exp(\overline{\ln \Delta}) = 2J_{\text{max}} \exp(-\overline{\Gamma})$, where

$$\Gamma = \ln \left(\frac{2J_{\text{max}}}{\Delta} \right) = \ln \left(\frac{2e^{1-\delta}}{\Delta} \right) \quad (46)$$

(analogously for Γ_{LB}). From the leading finite-size behavior [13],

$$\overline{\Gamma} = \text{const} + z \ln L, \quad (47)$$

we obtain the effective dynamical exponent z . Repeating this procedure for different distances from criticality δ , we then obtain $z = z(\delta)$ and compare with the analytical result (45).

We start with moderate size lattices (up to $L = 2500$) and $h_s = 0$. In Fig. 11 (top panel), $\overline{\Gamma}$ and $\overline{\Gamma}_{\text{LB}}$ (averaged over 10^6 distinct disorder configurations) are plotted as functions of L for different values of δ . As in the critical case, we see no difference between the exact (open circles) and the LB estimate (\times symbols). A best fit of (47) to the data within the range $1950 \leq L \leq 2500$ (dashed box) provides an estimate for the exponent z and z_{LB} .

It is well-known that estimates of critical exponents obtained directly from best fits of a leading finite-size behavior may contain systematic errors. Mainly, this is because the lattice size L is not sufficiently large to reach the asymptotic regime where (47) is valid. An interesting strategy to detect whether such lattices reached the asymptotic regime is by using the finite-size estimate

$$z(L, L') = \frac{\overline{\Gamma}_L - \overline{\Gamma}_{L'}}{\ln(L/L')}, \quad (48)$$

with $L' = L - \Delta L$ and fixed difference ΔL . The estimate (48) tends towards the exact value of z as $L \rightarrow \infty$. In Fig. 11 (middle panel), we plot $z(L, L')$ and $z_{\text{LB}}(L, L')$ as a function of L for fixed $\Delta L = 25$. Clearly, system sizes up to $L = 2500$ are enough for the estimation of

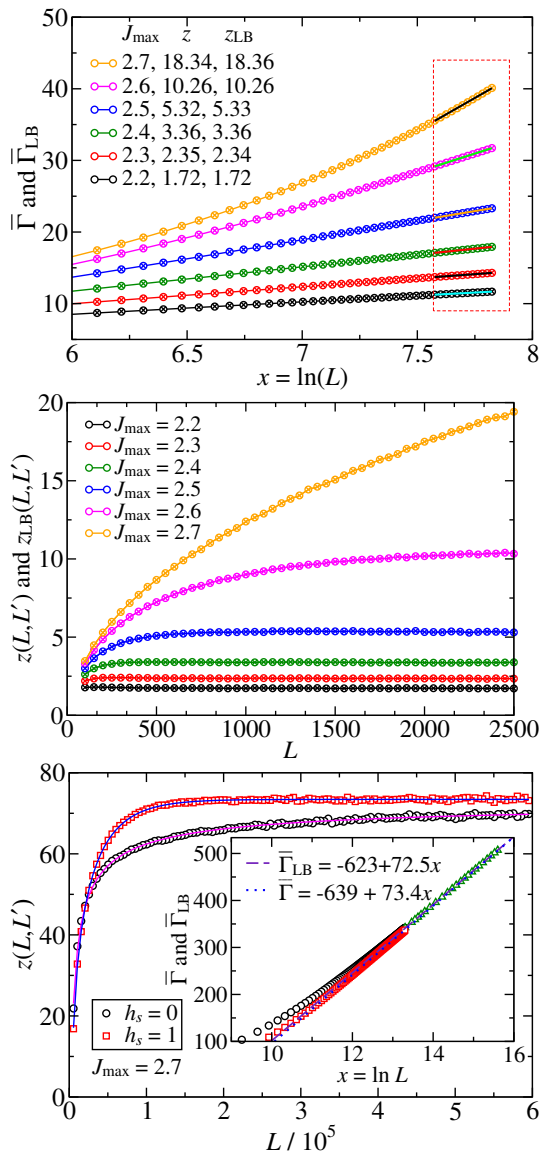


Figure 11. Top: The typical value of the mass gap $\bar{\Gamma}$ (46) (open circles) and the corresponding Laguerre's bound estimate $\bar{\Gamma}_{LB}$ (\times symbols), as functions of lattice size L (up to $L = 2500$) for the quantum Ising chain (3) with $h_s = 0$ and for various distances from criticality $\delta = 1 - \ln J_{\max}$ (different colors), $J_{\max} = 2.2, \dots, 2.7$ from bottom to top. Standard linear fits are restricted to within the dashed box region (solid lines), and the slopes are provided in the figure. Middle: The corresponding finite-size estimator $z(L, L')$ (48) as a function of L for fixed $\Delta L = 25$. As in the top panel open circles and \times symbols refer to z and z_{LB} , respectively. In both panels, the error bars are smaller than the symbol sizes. Bottom: The estimator $z(L, L')$ for system sizes up to $L = 6 \times 10^5$, $J_{\max} = 2.7$ (corresponding to $\delta = 6.7 \times 10^{-3}$), and $h_s = 0$ (black circles) and $h_s = 1$ (red squares). Solid lines are the fittings to Eqs. (49) and (50) (see text). The inset shows $\bar{\Gamma}$ (for $L < 6 \times 10^5$, circles and squares) from which the main panel was derived, see Eq. (48). In addition, $z_{LB}(L, L')$ (green triangles) is plotted for sizes $6 \times 10^5 < L < 6 \times 10^6$. Linear fits to the data are provided in the figure. Each data point is obtained by averaging over 10^6 (top and middle) 10^4 (bottom) different samples.

z for $J_{\max} < 2.5$ ($\delta \gtrsim 0.084$). Larger system sizes are, however, required for estimating z closer to criticality.

In Fig. 11 (bottom panel), we show the estimator $z(L, L')$ for chain sizes up to $L = 6 \times 10^5$, $\Delta L = 25$, $J_{\max} = 2.7$ (distance from criticality $\delta \approx 0.00675$), and $h_s = 0$ and 1. While $L \sim 6 \times 10^5$ is enough for estimating z for the case $h_s = 1$, such system size is still not enough for the obtaining z in the standard random transverse-field Ising chain ($h_s = 0$). As at criticality (see Fig. 10), such differences in the finite-size corrections for the models (3) with $h_s = 0$ and $h_s = 1$ are surprising. To obtain a reliable estimate of z for the case $h_s = 0$, we plot $\bar{\Gamma}_{LB}$ versus L for even larger system sizes, up to 6×10^6 , see inset of the bottom panel of Fig. 11. We verified that the slope (the estimate for z) does not change for $L \gtrsim 10^6$.

Recently, it was numerically verified in Ref. 21 that a finite-size estimate for the dynamical exponent in the $h_s = 0$ case converges as

$$z_L = z_\infty - A \frac{\ln^b L}{L}, \quad (49)$$

where A and b are δ -dependent fitting parameters and z_∞ is the SDRG prediction (45). We verify that (49) fits our data for $z(L, L')$ satisfactorily with $A = 9.90$ and $b = 4.75$ (see the magenta solid line fitting the circles in the bottom panel of Fig. 11). Allowing z_∞ to be a fitting parameter, we obtain $z_\infty = 73.146$ (the analytic prediction being 73.428), $A = 12.80$ and $b = 4.64$. A power-law fitting function of type AL^{-b} (without the logarithmic correction) is very poor. Interestingly, (49) fits our data for $h_s = 1$ very poorly. Instead, we verify that

$$z_L = z_\infty - A \frac{e^{-L/\zeta}}{L^b}, \quad (50)$$

fits our data remarkably well (see the blue solid line fitting the squares in the bottom panel of Fig. 11). The fitting parameters are $z_\infty = 73.431$, $A = 863$, $\zeta = 42719$ and $b = 0.30$. We verified that a power-law fitting is very poor. Evidently, this raise the question of the length scale ζ which we leave as an open question.

In Fig. 12, we plot the effective dynamical exponent z as a function of the distance from criticality δ for the cases $h_s = 0$ and $h_s = 1$. Our data agrees remarkably well with the analytical prediction (45) (dotted line). We remark that the dynamical exponent obtained from the finite-size analysis of Δ_{LB} agrees remarkably well with that obtain from the exact value of the mass gap Δ .

VI. CONCLUSIONS

We present a numerical method that proves to be quite effective for calculating the low-lying eigenspectrum of a general family of free-fermionic and parafermionic quantum chains with small values of mass gaps. The method is suitable for free-particle quantum chains whose eigenenergies are given in terms of the zeros of polynomials with simple recurrence relations. Models in this

class are the multi-spin interacting generalizations of the Ising and XY quantum chains as well as any generalization of the tight-binding model. The computing time for the mass gap evaluation grows only linearly with the number of sites of the quantum chain. This happens because we only need to calculate a fixed number of coefficients of the associated polynomial, regardless of the system's size. For higher dimensional models or models with long-range interactions, however, the characteristic polynomial is not efficiently generated in general and, thus, our method is not guaranteed to be more than the standard exact diagonalization.

As a benchmark, we mention that the method allows the mass gap evaluation of the standard Ising quantum chain at its critical point and with a number of sites $L = 100, 200, \dots, 1.2 \times 10^6$ (12 000 mass gaps) in only two seconds of a CPU time in a regular portable computer.

An important ingredient of our method is the use of the LB for the largest zero of polynomials. This bound allows us a good initial guess in the numerical procedure of searching for the largest root of the polynomial, giving us the mass gap. Actually, for the multi-spin interacting Ising quantum chains at their multi-critical point we show analytically that the gap obtained directly from the LB has the same leading finite-size behavior as the exact mass gap, rendering us the exact value for the dynamical critical exponent (35). As discussed in Sec. IV D, the success of the LB stems from the fact that, at criticality or in gapless phases, the largest zero of the characteristic polynomial separates from the other roots and dominates the value of the LB.

We believe that the method we propose in this paper will be especially relevant for the case of random systems, where a large number of mass gaps evaluations are necessary to achieve statistical accuracy.

We considered random transverse-field Ising chains at the critical point and inside the Griffiths paramagnetic

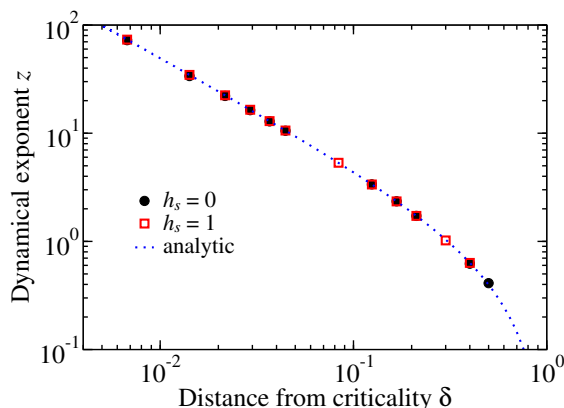


Figure 12. The dynamical exponent z as a function of the distance from criticality δ in the Griffiths paramagnetic phase $0 < \delta < 1$ of the random transverse-field Ising chain (3) for the cases with ($h_s = 1$) and without ($h_s = 0$) the longitudinal surface field. The dotted line is the analytic prediction (45).

phase. The effective dynamical critical exponent in the Griffiths phase diverges toward the critical point. The numerically exact evaluation of this exponent around the critical point is a quite difficult problem for standard numerical methods since numerical instabilities appear already in chains of moderate sizes. Our calculations for lattice sizes up to $L \sim 10^6$ give us a prediction that agrees with the early ones of the SDRG method [13] and additional analytical results [20].

The results obtained directly from the LB give us, surprisingly, quite good estimates also in the case of random systems, and become asymptotic exact as $L \rightarrow \infty$. The computation time of the LB and SDRG are of the same order, both methods are complementary for the class of models we considered in this paper. A nice surprise of this paper is the demonstration that the LB, initially thought to be just a convenient initial guess for the method, turned out to be a *quite precise approximation of the exact result*, being more precise than the standard SDRG method.

As a final remark, since the analytical form of the LB is simple, this opens the exciting possibility of obtaining analytical results for quenched disordered systems.

ACKNOWLEDGMENTS

This paper was supported in part by the Brazilian agencies FAPESP and CNPq.

Appendix A: The strong-disorder renormalization-group method

In this appendix, we simply review the SDRG decimation procedure [13] for the transverse-field Ising chain (3) without the surface longitudinal field ($h_s = 0$). Later, we generalize for finite h_s .

The SDRG procedure states that one has to search for the strongest coupling or transverse field in the chain $\Omega = \max\{J_i, h_i\}$. In the case of a transverse field, say, h_2 , the corresponding spin is removed from the system and the neighbors are connected via a renormalized coupling constant equal to

$$\tilde{J} = \frac{J_1 J_2}{h_2}. \quad (\text{A1})$$

On the other hand, if $\Omega = J_2$, then the spins sharing that coupling are fused into a single one. The couplings with the neighbor spins do not change. The local transverse field, however, is renormalized to

$$\tilde{h} = \frac{h_1 h_2}{J_2}. \quad (\text{A2})$$

To obtain the low-energy physics, one iterates the above procedure until a desired energy scale Ω . For the mass

gap, one iterates this procedure until a single spin remains. The effective Hamiltonian is simply $-\tilde{h}_{\text{final}}\sigma^x$, and the mass gap is, thus,

$$\Delta_{\text{SDRG}} = 2\tilde{h}_{\text{final}}. \quad (\text{A3})$$

We note that, for the purpose of computing Δ_{SDRG} , there is no need to perform the above procedure following the rule of searching for the strongest J or h . Since Eqs. (A1) and (A2) produce only smaller renormalized energy scales, the decimation procedure can be performed locally. For instance, if h_m is greater than J_m and J_{m+1} , it is then guaranteed that h_m will be, at some point, decimated since J_m and J_{m+1} can only be renormalized to smaller values. Therefore, the procedure simply sweeps the entire chain, decimating h_m (J_m) if J_m and J_{m+1} (h_m and h_{m+1}) and renormalizing the couplings (fields) accordingly to (A1) [(A2)]. The smallest decimated field $\tilde{h}_{<}$ is then the final field decimated in the usual procedure $\tilde{h}_{<} = \tilde{h}_{\text{final}}$ and, thus, provides the mass gap Δ_{SDRG} in Eq. (A3). Note that this is a procedure that increases linearly with system size, as shown in Fig. 8.

In Fig. 13 we show, for the sake of a direct comparison, the values of Δ (computed exactly as explained in Sec. III) and of the estimates Δ_{LB} and Δ_{SDRG} (A3). We pick up to random sequences $\{J_i\}$ of size $L_{\text{max}} = 3 \times 10^5$. Then, we compute Δ , Δ_{LB} , and Δ_{SDRG} for a system of size $5 \times 10^4 \leq L \leq L_{\text{max}}$, picking up the couplings $\{J_i\}$ from $i = 1$ to L . We see from these figures that the exact gaps (red squares) stay almost unchanged for large plateaus of lattice sizes $L_1 \leq L \leq L_2$. This can be easily understood within the SDRG decimation procedure described above. For each particular $\{J_i\}$ ($1 \leq i \leq L_1$), the smallest decimated field yielding the mass gap, $\tilde{h}_{<}$, happens already for a smaller lattice site $L < L_1$. It is remarkable that, indeed, the exact mass gap follows the SDRG prediction in almost all chains. This provides further confidence in the infinite-randomness criticality provided by the SDRG method. More importantly, note that the LB estimate also closely follows the SDRG prediction. It is remarkable that such a step-wise curve can be obtained from the ‘‘simple’’ analytic result (25).

We now generalize the SDRG decimation procedure to include the surface field h_s in (3). One simple way is the following. Notice that the spectrum of (3) is the same as

$$H = - \sum_{i=1}^L h_i \sigma_i^x - \sum_{i=1}^{L-1} J_i \sigma_i^z \sigma_{i+1}^z - h_s \sigma_L^z \sigma_{L+1}^z, \quad (\text{A4})$$

i.e., a transverse field Ising chains with open boundary conditions, just like (3), however, with one additional spin (thus, the degeneracy is double of the original Hamiltonian) at site $L+1$ coupled to the spin at site L through a coupling constant $J_L = h_s$. In addition, the transverse field on this additional spin is vanishing ($h_{L+1} = 0$). Since (A4) has the same operator content as (3), the above procedure can be directly used. The only caveat is

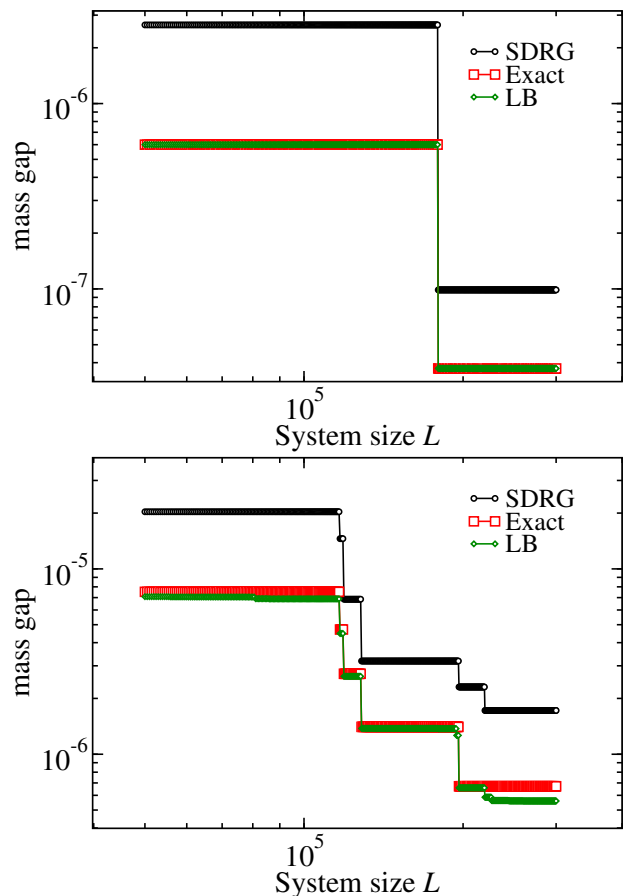


Figure 13. The mass gap Δ and the corresponding Laguerre’s bound and SDRG estimates of two randomly chosen configurations of couplings $\{J_i\}$ of the system Hamiltonian (3) with $h_s = 0$ and $\delta = 0$, see Eq. (42). These quantities are computed considering the sequence $\{J_i\}$ from 1 to L ; we vary the lattice sizes from $L = 50\,000$ to $300\,000$.

when decimating $J_L = h_s$. A direct application of (A2) leads to $\tilde{h} = 0$ since $h_{L+1} = 0$. Reiterating the procedure yields $\tilde{h}_{\text{final}} = \tilde{h}_{<} = 0$. This is a consequence of the ground state being doubly degenerate.

To solve this problem, one needs to consider the two-site problem $H_0 = -h_L \sigma_L^x - J_L \sigma_L^z \sigma_{L+1}^z$. The corresponding spectrum is $\pm \sqrt{h_L^2 + J_L^2}$ with each state being doubly degenerate. Treating $H_1 = -J_{L-1} \sigma_{L-1}^z \sigma_L^z$ as a perturbation to H_0 , we find, in first order of perturbation theory, an effective Hamiltonian $\tilde{H} = -\tilde{J}_{L-1} \sigma_{L-1}^z \tilde{\sigma}_L^z$ with

$$\tilde{J}_{L-1} = \frac{J_{L-1} J_L}{\sqrt{h_L^2 + J_L^2}}, \quad (\text{A5})$$

and $\tilde{\sigma}_L$ being a new effective spin describing the low-lying behavior of the decimated spins σ_L and σ_{L+1} . Notice that the renormalized Hamiltonian is the same as before but with one less spin and a new surface longitudinal field $\tilde{h}_s = \tilde{J}_{L-1}$ in (A5). Importantly, the renormalized $\tilde{J}_{L-1} < J_{L-1}$ and, thus, the decimation procedure can be carried out locally as in the usual case. Finally, the

mass gap associated with decimating J_L is $\sqrt{h_L^2 + J_L^2}$. Therefore, the mass gap Eq. (A3) generalizes to

$$\Delta_{\text{SDRG}} = 2\sqrt{\tilde{h}_{\text{final}}^2 + \tilde{J}_{\text{final}}^2}. \quad (\text{A6})$$

Another way is generalizing the SDRG procedure to Ising chains with longitudinal and transverse fields

$$H = - \sum_i J_i \sigma_i^z \sigma_{i+1}^z + h_i \sigma_i^x + B_i \sigma_i^z. \quad (\text{A7})$$

(We are then interested in the particular case that $B_i = h_s \delta_{i,L}$.) For uncorrelated disorder variables $\{J_i, h_i, B_i\}$, the SDRG decimation procedure can be generalized following the reasoning of Ref. 13. We search for the strongest coupling constant and total field in the chain $\Omega = \max\{J_i, g_i\}$, with $g_i = \sqrt{h_i^2 + B_i^2}$. In the case of a total field, say, g_2 , the corresponding spin is removed from the system and the neighbors are connected via a renormalized coupling constant equal to

$$\tilde{J} = \frac{J_1 J_2 h_2^2}{g_2^3}. \quad (\text{A8})$$

In addition, the neighboring longitudinal fields are also renormalized to

$$\tilde{B}_1 = B_1 + \frac{J_1 B_2}{g_2} \text{ and } \tilde{B}_3 = B_3 + \frac{J_2 B_2}{g_2}. \quad (\text{A9})$$

Notice that Eqs. (A8) and (A9) recover (A1) for $B_i = 0$. On the other hand, if $\Omega = J_2$, then the spins sharing that coupling are fused into a single one. The couplings with the neighbor spins do not change. The local field, however, is renormalized to

$$\tilde{h} = \frac{h_1 h_2}{J_2} \text{ and } \tilde{B} = B_1 + B_2. \quad (\text{A10})$$

As for the usual case, the mass gap is obtained by iterating this procedure until a single spin remains. The effective Hamiltonian is simply $-\tilde{h}_{\text{final}} \sigma^x - \tilde{B}_{\text{final}} \sigma^z$, and the mass gap is, thus,

$$\Delta_{\text{SDRG}} = 2\sqrt{\tilde{h}_{\text{final}}^2 + \tilde{B}_{\text{final}}^2}, \quad (\text{A11})$$

which recovers (A6).

Finally, we note that an analysis of the effects of the longitudinal field in the bulk was provided in Ref. 22.

-
- [1] T. D. Schultz, D. C. Mattis, and E. H. Lieb, *Rev. Mod. Phys.* **36**, 856 (1964).
- [2] P. Pfeuty, *Annals of Physics* **57**, 79 (1970).
- [3] R. J. Baxter, *Physics Letters A* **140**, 155 (1989).
- [4] P. Fendley, *Journal of Physics A: Mathematical and Theoretical* **47**, 075001 (2014).
- [5] F. C. Alcaraz and R. A. Pimenta, *Phys. Rev. B* **102**, 121101 (2020).
- [6] F. C. Alcaraz and R. A. Pimenta, *Phys. Rev. B* **102**, 235170 (2020).
- [7] Y. Zhao, F. Andraschko, and J. Sirker, *Phys. Rev. B* **93**, 205146 (2016).
- [8] G. Roósz, Y.-C. Lin, and F. Iglói, *New Journal of Physics* **19**, 023055 (2017).
- [9] J. C. Getelina and J. A. Hoyos, *Eur. Phys. J. B* **93**, 2 (2020).
- [10] Q. I. Rahman and G. Schmeisser, *Analytic Theory of Polynomials*, edited by H. G. Dales and P. M. Neumann, London Mathematical Society Monographs New Series, Vol. 26 (Clarendon Press, Oxford, 2002).
- [11] M. Marden, *Geometry of Polynomials*, 2nd ed., Mathematical Surveys and Monographs, Vol. 3 (American Mathematical Society, Providence, Rhode Island, 1966).
- [12] S. T. Jensen and G. P. H. Styan, “Some comments and a bibliography on the laguerre-samuelson inequality with extensions and applications in statistics and matrix theory,” in *Analytic and Geometric Inequalities and Applications*, edited by T. M. Rassias and H. M. Srivastava (Springer Netherlands, Dordrecht, 1999) pp. 151–181.
- [13] D. S. Fisher, *Phys. Rev. B* **51**, 6411 (1995).
- [14] P. Fendley, *Journal of Physics A: Mathematical and Theoretical* **52**, 335002 (2019).
- [15] S. J. Elman, A. Chapman, and S. T. Flammia, *Commun. Math. Phys.* **388**, 969 (2021).
- [16] V. P. Spiridonov, S. Tsujimoto, and A. S. Zhedanov, *Commun. Math. Phys.* **272**, 139 (2007).
- [17] X.-K. Chang, X.-B. Hu, J. Szmigielski, and A. S. Zhedanov, *Commun. Math. Phys.* **377**, 387 (2020).
- [18] D. S. Fisher and A. P. Young, *Phys. Rev. B* **58**, 9131 (1998).
- [19] H. J. Mard, J. A. Hoyos, E. Miranda, and V. Dobrosavljević, *Phys. Rev. B* **90**, 125141 (2014).
- [20] F. Iglói, R. Juhász, and P. Lajkó, *Phys. Rev. Lett.* **86**, 1343 (2001).
- [21] I. A. Kovács, T. Pető, and F. Iglói, *Phys. Rev. Research* **3**, 033140 (2021).
- [22] P. Lajkó, J.-C. A. d’Auriac, H. Rieger, and F. Iglói, *Phys. Rev. B* **101**, 024203 (2020).